

Behavior of Primary Radicals during Thermal Degradation of Poly(Methyl Methacrylate)*

Takashi Kashiwagi, Atsushi Inabi[‡]

Center for Fire Research, National Bureau of Standards,
Gaithersburg, Maryland 20899, USA

&

Anthony Hamins

Chemistry Department, George Washington University, Washington,
DC 20052, USA

(Received 10 August 1988; accepted 11 October 1988)

ABSTRACT

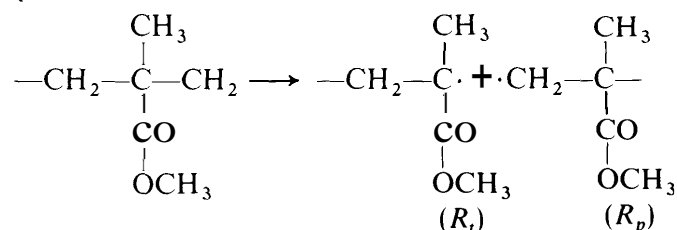
The behavior of the primary radicals, formed from the random scission of anionically polymerized poly(methyl methacrylate), PMMA, during thermal degradation is investigated by a theoretical and experimental study. The theoretically calculated relationship between the degree of polymerization and the conversion agrees well with the experimentally determined relationship if the random scission produces one polymer radical and one polymer molecule with an unsaturated bond at a chain end. It is proposed that the primary radical rearranges to form the polymer molecule with the unsaturated bond at a chain end. Two different degradation paths for this rearrangement are proposed via β scission at the C—C bond of the pendant group instead of β scission, as previously thought, at the backbone C—C bond. The products from the proposed degradation paths are CO, CO₂, CH₃OH, and CH₄. The products for anionically polymerized PMMA samples with three different values of initial molecular weight are measured by a mass spectrometer. The quantities of CO and CO₂ are observed to decrease with an increase in initial molecular weight. This confirms that the two proposed degradation paths for the thermal degradation of PMMA are quite plausible.

* Contribution from the National Bureau of Standards, not subject to copyright.

[‡] Guest worker from National Research Institute for Pollution and Resources, Tsukuba, Japan.

INTRODUCTION

In our previous study,¹ the effects of initial molecular weight on the thermal degradation of anionically polymerized PMMA were studied by close coordination between theoretical modeling and experimental data in order to improve the understanding of the complex thermal degradation mechanism. This well characterized polymer was selected so that theoretically calculated results using known parameters could be quantitatively compared with experimental data. In the previous model the same depropagation rate via β scission from both primary and tertiary radicals generated from the random scission at backbone C—C bonds was assumed. Although the theoretically calculated activation energies for a global reaction based on weight loss rates agreed reasonably well with the experimentally determined activation energies, the theoretical estimates showed an inconsistency in the prediction of the value of the average zip length and also did not agree well with the experimentally determined weight loss rates as a function of temperature under dynamic heating conditions. Since the calculated results were reasonably close to the experimental data, it is expected that the modification is not a major one. After the degradation scheme was reviewed, the assumption of equal reactivities of the primary radicals (R_p) and tertiary radicals (R_t)



which are formed after the random scission at backbone C—C bonds, was discussed. A similar question was raised for the degradation of poly(α -methylstyrene), P α MS,² and polystyrene, PS.³ In these previous studies, two possible degradation paths were considered for the two radicals formed from the random scission initiation: (1) disproportionation termination between the two radicals to form two polymer molecules,³ and (2) intermolecular abstraction of hydrogen by the primary radical and β scission from the tertiary radical.² Since there is no benzene-induced resonance stability and no tertiary hydrogens in the PMMA structure, the above proposed second path for the primary radical may not occur during the degradation of PMMA. The first path may occur because it is known that the disproportionation termination occurs during the radical polymerization process of PMMA.⁴ This point is pursued in this study in order to clarify the behavior of the primary radical.

This study consists of three parts: first, an elucidation of the behavior of the primary radical; secondly, a theoretical calculation of changes in molecular weight distribution and weight loss rates based on the above elucidation and a direct comparison of the calculated results with experimental data; and, thirdly, an experimental confirmation of the above elucidation.

PROBABLE BEHAVIOR OF THE PRIMARY RADICAL

The probable behavior of the primary radical created from the scission at backbone C–C bonds is elucidated in this section. The previously measured relationship between the number average degree of polymerization of the sample residue, X/X_0 (X is the initial number average degree of polymerization), and the conversion, $1 - W/W_0$ (W_0 is the initial sample weight), for three different initial molecular weights of anionically polymerized PMMA samples is shown in Fig. 1.¹ The first model (Model I),¹ based on equal reactivities of the primary and tertiary radicals, can be expressed as:



where M_n is a polymer molecule with a degree of polymerization of n and R ,

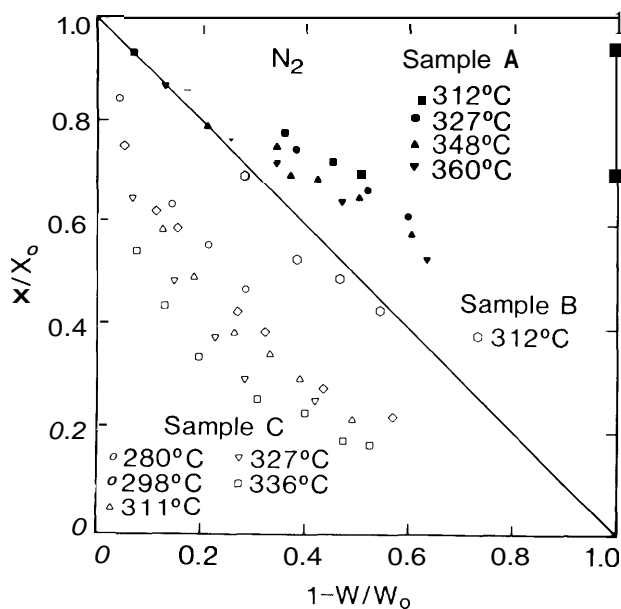


Fig. 1. Normalized number average degree of polymerization of the sample residue plotted against the conversion, $1 - W/W_0$, at various temperatures. The solid line is 45° diagonal line. (X_0 value **A**: 315, **B**: 1250, **C**: 5690).

is a polymer radical with a degree of polymerization x . The calculated results based on this reaction scheme underestimate the relationship between the number average degree of polymerization and the conversion for the lowest initial molecular weight PMMA sample, sample A.¹ This suggests that at least one polymer molecule would be formed to reduce the degree of polymerization. There are two possible reaction schemes to generate one or two polymer molecules:



where M_x^* is a thermally less stable polymer molecule than M_x and it contains a weak linkage such as an unsaturated bond at the polymer end.⁴ The reaction scheme (3) could be considered to be the result of a disproportionation termination reaction between the primary radical and the tertiary radical similar to the case for PS.³ At this moment, the detailed reaction scheme for reaction (2) is not speculated upon and it is considered merely to be an artificial reaction scheme which creates one molecule and one radical from the scission.

The model based on reaction scheme (2) with depropagation and termination reactions is developed for the calculation of changes in degree of polymerization and weight of a sample residue. The detailed derivation of the model is described in the Appendix of this paper. The calculated results for the relationship between changes in degree of polymerization and conversion are shown in Fig. 2. As derived in the Appendix, as $Z/X_0 \rightarrow \infty$, where Z/X_0 is average zip length (Z is the ratio of depropagation rate to termination rate), the relationship becomes

$$1 - X/X_0 = 1 - W/W_0$$

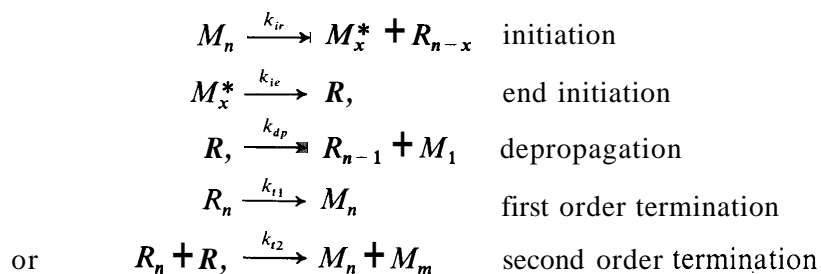
which shows that the relationship based on reaction scheme (2) does not cross over the 45° diagonal line for any value of Z/X_0 . Since more polymer molecules are generated from reaction scheme (3) than from reaction scheme (2), it is expected that the relationship between the number average degree of polymerization and the conversion calculated with reaction scheme (3) should be lower than that with reaction scheme (2) in Fig. 2. Furthermore, it cannot cross over the 45° diagonal line for any value of Z/X_0 . The experimentally obtained relationship shown in Fig. 1 indicates clearly that this relationship for sample A ($X_0 = 315$) crosses over the 45° diagonal line. The value of Z/X_0 for sample A is estimated to be between 5 and 10. Therefore, it is concluded that the two reaction schemes (2) and (3) do not contribute appreciably during the thermal degradation of PMMA.

Since the relationship calculated with reaction scheme (1) for sample A overestimates the experimentally obtained relationship and that with reaction scheme (2) underestimates it, it appears that the correct reaction

The above reaction is the scission at the weakest β location on the primary radical site instead of at the backbone C—C bond as in reaction scheme (1). It is estimated that the activation energy of the above β scission is about 10kJ/mol (2–3kcal/mol) less than that of the β scission at the backbone C—C bond? The radicals $\cdot\text{OCH}_3$ and $\cdot\text{CH}_3$ might abstract hydrogen to form CH_3OH and CH_4 , quench at walls, or evolve without further reactions. For P α MS, the above proposed β position from the primary radical site is —C—Ph which is more stable than the proposed β scission for PMMA due to the resonance effect of the benzene ring. Therefore, the proposed β scission would not occur for P α MS. For PS, intermolecular or intramolecular hydrogen transfer is favored over the proposed β scission due to the existence of tertiary hydrogens and the resonance stability of the benzene ring in the PS structure. The model based on the proposed β scission is described in the next section and is used to calculate changes in molecular weight and conversion during the thermal degradation of anionically polymerized PMMA samples.

THE MODEL BASED ON THE PROPOSED REACTION SCHEME (MODEL 11)

The proposed model is:



where k_{ir} , k_{ie} , k_{dp} , k_{t1} , and k_{t2} are rate constants for random initiation, end initiation, depropagation, first and second order termination reactions, respectively. Similar to Model I, monomer is evolved in this model, as are the radicals $\cdot\text{OCH}_3$ and $\cdot\text{CH}_3$. Then, the governing equations are:

$$d[M_n^0]V/dt = -k_{ir}(n-1)[M_n^0]V + k_{ie}\beta[R_n]V \quad (7)$$

$$d[M_n^*]V/dt = -k_{ie}[M_n^*]V - k_{ir}(n-1)[M_n^*]V + k_{t1} \sum_{i=n+1}^{\infty} [M_i]V \quad (8)$$

$$\begin{aligned} d[R_n]V/dt = & k_{ie}[M_n^*]V + k_{ir} \sum_{i=n+1}^{\infty} [M_i]V \\ & + k_{dp}([R_{n+1}]V - [R_n]V) - k_t\beta[R_n]V \end{aligned} \quad (9)$$

$$d[R_1]V/dt = k_{dp}[R_2]V + k_{ir} \sum_{n=2}^{\infty} [M_n]V - k_t\beta[R_1]V \quad (10)$$

where:

$$\beta = \begin{cases} 1 & \text{for first order termination} \\ \sum_{n=1}^{\infty} [R_n] & \text{for second order termination} \end{cases}$$

$$[M_n] = [M_n^0] + [M_n^*]$$

where $[M_n^0]$ denotes the concentration of polymer molecules with a degree of polymerization n without a double bond at the chain end and $[M_n^*]$ is the polymer molecule concentration with a double bond at the terminal end of the chain. Correspondingly, $[R_n]$ is the Concentration of polymer radicals with an n th degree of polymerization. Vis the volume of the sample residue during the degradation. The addition of eqn (7) with eqn (8) gives:

$$d[M_n]V/dt = -k_{ie}[M_n^*]V - k_{ir}(n-1)[M_n]V + k_{ir} \sum_{i=n+1}^{\infty} [M_i]V + k_t\beta[R_n]V \quad (11)$$

Then, the rate of change in sample volume becomes:

$$dV/dt = \left(d \sum_{n=2}^{\infty} n[M_n]V/dt \right) (m_0/\rho) \quad (12)$$

where ρ is the density of the sample which is assumed to be a constant during the degradation and m_0 is the molecular weight of a monomer unit. Multiplying by ρ on both sides of eqn (12), the rate of change in the sample weight can be determined. As discussed in detail in our previous study, ' the assumption of steady-state radical concentration is quite reasonable for the thermal degradation of the above three PMMA samples. Then, the steady-state radical concentration can be derived from eqns (7) and (8) with the

steady-state form of eqn (9) as:

$$[R_n] = \frac{Z_{per}Z'}{(1+Z)} \sum_{i=n}^{\infty} \left[\left(\frac{Z}{1+Z} \right)^{i-n} [M_i^*] \right] + \frac{Z'}{(1+Z)} \sum_{j=n+1}^{\infty} \left[\left(\frac{Z}{1+Z} \right)^{j-(n+1)} \sum_{i=j}^{\infty} [M_i] \right] \quad (13)$$

where:

$$Z = k_d/(k_t\beta) \quad Z' = k_{ir}/(k_t\beta) \quad Z_{per} = k_{ie}/k_{ir}$$

Substituting the above expression of $[R_n]$ into eqns (8) and (11), they become:

$$d[M_n^*]V/dt = Z_{per}[M_n^*]V - (n-1)[M_n^*]V + \sum_{i=n+1}^{\infty} [M_i]V \quad (14)$$

$$d[M_n]V/dt = Z_{per}[M_n^*]V - (n-1)[M_n]V + \sum_{i=n+1}^{\infty} [M_i]V + \frac{Z_{per}}{(1+Z)} \sum_{i=n}^{\infty} \left[\frac{Z}{1+Z} \right]^{i-n} [M_i^*]V + \frac{1}{1+Z} \sum_{j=n+1}^{\infty} \left[\left\{ \frac{Z}{1+Z} \right\}^{j-(n+1)} \sum_{i=j}^{\infty} [M_i]V \right] \quad (15)$$

The initial molecular weight distribution of the sample must be specified in order to solve the above differential equations. In this study, experimentally determined number average molecular weights for the three samples expressed by a logarithmic normal distribution are used as an initial condition. For the integration of the ordinary differential equations of eqns (12), (14), and (15), the integral method of Shampine⁵ is used. The maximum lengths of polymer molecules and radicals are assumed to be ten times that of the initial degree of polymerization instead of infinity as described in the above equations.

In Model I (reaction scheme (1)), the degree of polymerization and the weight of the sample can be determined with only one parameter, Z , by solving the non-dimensionalized differential equations.⁷ However, in Model II, the additional parameter, Z_{per} , is needed as described by eqns (14) and (15). Therefore, the determination of kinetic constants for the two parameters, Z and Z_{per} , in Model II becomes more complex than that in

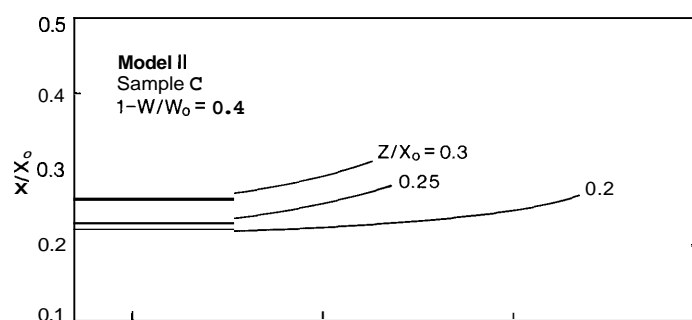


Fig. 3. Theoretically calculated normalized degree of polymerization plotted against Z_{per} at various values of Z/X_0 for sample C.

Model I. Since Z and Z_{per} are defined by kinetics only ($Z = k_d/(k_t\beta)$, $Z_{per} = k_{ie}/k_{ir}$), at the same degradation temperature the values of these parameters should be equal to each other for the same value of conversion, regardless of the initial molecular weight of the sample.

It is demonstrated here how to determine the unique pair of Z and Z_{per} values using the experimental results shown in Fig. 1. In order to obtain the relationship between Z and Z_{per} , first the relationship between X/X_0 and Z_{per} for various values of Z/X_0 is calculated for each sample. Typical results of this relationship are shown in Fig. 3 for sample C for a conversion of 0.4. If the value of X/X_0 is determined from the experimental data with the same conversion for each sample, three pairs of corresponding values of Z/X_0 and Z_{per} can be determined by using the three curves shown in Fig. 3. At 327°C the value of X/X_0 for sample C at a conversion of 0.4 is 0.26 as determined from the results shown in Fig. 1. Three pairs of the corresponding values of Z/X_0 and Z_{per} are (0.3, 190), (0.25, 1030), and (0.2, 19000). The value of Z can be determined from the known value of X_0 (5690 for sample C). Then, the relationship between Z and Z_{per} can be plotted as shown in Fig. 4. The same procedure is repeated for samples A and B for a conversion of 0.4 and a temperature of 327°C. The relationship obtained for each sample is shown in Fig. 4. If the scatter in data is much less than those shown in Fig. 1, the three curves should meet at one point corresponding to the unique pair of Z and Z_{per} values. (The relationship between Z/X_0 and Z_{per} is very sensitive to the experimentally determined value of X/X_0 as shown in Fig. 3.) The value of 500 for Z_{per} and the corresponding value of 1500 for Z are selected from the results shown in Fig. 4 at a temperature of 327°C and a conversion of 0.4.

Although the same procedure can be repeated for various other temperatures described in Fig. 1, another approach is used to determine the pairs of Z/X_0 and Z_{per} values at different temperatures using the above

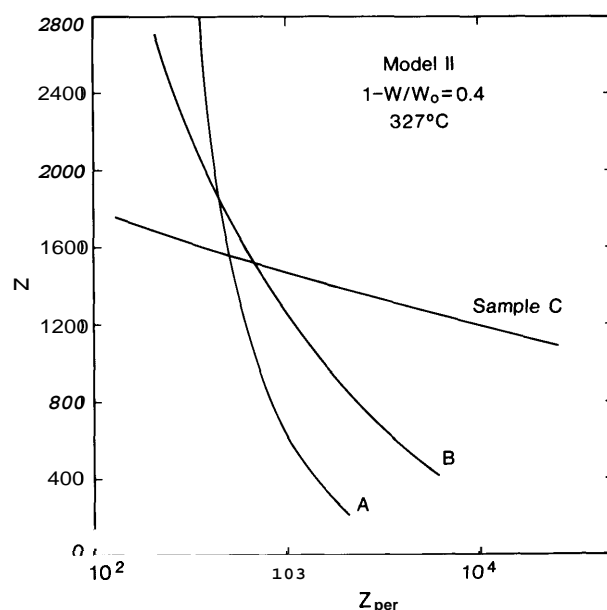


Fig. 4. Theoretically calculated number average zip length plotted against Z_{per} for the three samples at 327°C .

determined value of Z_{per} at 327°C . This approach avoids the use of the relationship between Z/X_0 and Z_{per} which is highly sensitive to X/X_0 .

As defined in the beginning of this section, $Z_{per} (=k_{ie}/k_{ir})$ is the ratio of the end initiated rate constant to the random scission initiated rate constant. Although it is difficult to estimate the absolute rate of the end initiation, the activation energy of the end initiation with respect to that of the random scission initiation can be estimated with reasonable accuracy from the difference in bond strength between the two initiations. It is estimated that the activation energy of the end initiation (by β scission) from the double bond at the chain end is about 33kJ/mol (8kcal/mol) less than that of the random scission initiation.⁶ Then, Z_{per} can be expressed as:

$$Z_{per} = k_{ie}/k_{ir} = A_{ie}/A_{ir} \exp\{(E_{ie} - E_{ir})/RT\} = C \exp(8000/RT)$$

The value of the ratio of the two pre-exponential factors, C , for Z_{per} can be determined from the above determined value of Z_{per} ($=500$) at 327°C . Then, it becomes:

$$Z_{per} = 0.6 \exp(8000/RT) \quad (16)$$

Using this relationship, the effects of Z_{per} on the relationship between X/X_0 and Z/X_0 and also between τ ($\tau = k_{ir}t$) and Z/X_0 can be obtained and the results are plotted in Figs. 5(a) and 5(b), respectively. These results show

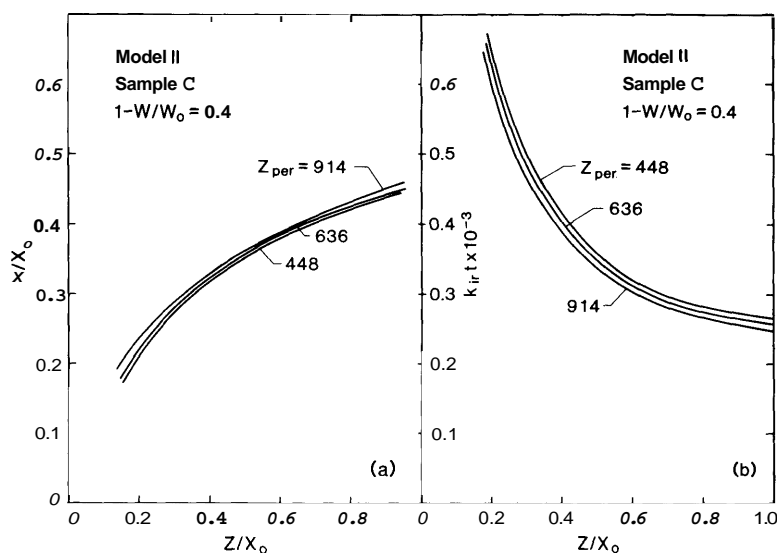


Fig. 5. Theoretically calculated relationships for sample C at various values of Z_{per} : (a) normalized number average degree of polymerization vs normalized average zip length, and (b) non-dimensionalized time vs normalized average zip length.

slight effects of Z_{per} on both relationships as expected from the results shown in Fig. 3.

The values of k_{ir} and Z for each degradation temperature are determined as follows: (1) the value of X/X_0 at the conversion of 0.4 is determined from the experimental results shown in Fig. 1 at the specific degradation temperature, (2) the value of Z_{per} at the specific degradation temperature is calculated from eqn (16), (3) using Fig. 5(a), the value of Z/X_0 corresponding to the above value of X/X_0 is determined with the value of Z_{per} (4) the value of $k_{ir}t$ corresponding to the values of Z/X_0 and Z_{per} is determined from Fig. 5(b), and (5) heating time, t , for the conversion at 0.4 is determined from the experimental results in a figure similar to Fig. 2 of our previous study. This procedure is repeated at each different degradation temperature corresponding to that shown in Fig. 1 at the same conversion. The Arrhenius plots of k_{ir} and Z determined from the above procedure are shown in Fig. 6 for samples **A** and **C**. There is a slight difference in the plots for k_{ir} and Z between the two samples, but the agreement between them is much better than that from Model I, especially for Z . The kinetic expressions for Z and k_{ir} are chosen from sample C as:

$$k_{ir} = 2.2 \times 10^8 \exp(-68000/RT) \quad (17)$$

$$Z = 0.18 \exp(11000/RT) \quad (18)$$

The activation energy for k_{ir} is almost the same in both Model I and Model

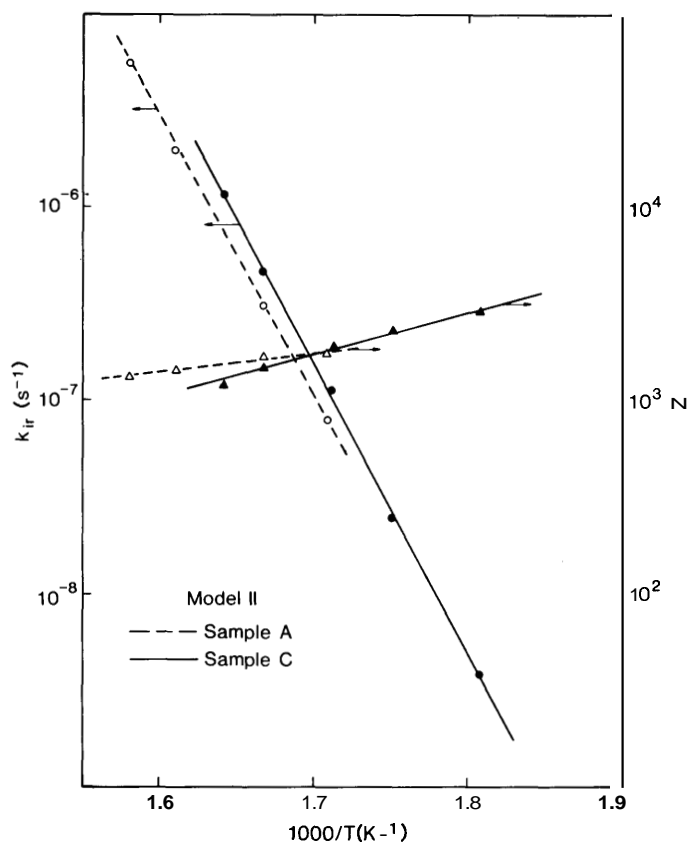


Fig. 6. Theoretically calculated Arrhenius plots of random scission initiation rate and of average zip length for samples A ($X_0 = 315$) and C (5690).

II while the activation energy for Z determined from Model II is about 40% larger than that determined from Model I (activation energies in eqns (17) and (18) are in kcal/mol).

The estimated value of the bond dissociation energy for the rupture of the backbone C—C bond for small molecules (gases) having a structure similar to PMMA is about 326 kJ/mol (78 kcal/mol) which is about 42 kJ/mol (10 kcal/mol) larger than the activation energy described by eqn (17). Although there is steric strain on the bonds caused by rigidity and conformation of the polymer molecule compared with small molecules, rearrangement of the primary radical also occurs. It is not clear at present what causes such a large difference in activation energy of the scission between the polymer molecule and small molecules.

The theoretically calculated relationships between X/X_0 and the conversion based on the two models are compared for samples A and C at different degradation temperatures and the results are shown in Fig. 7.

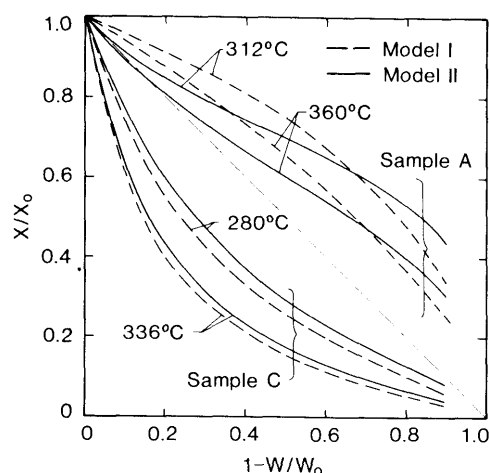


Fig. 7. Comparison of theoretically calculated relationships of normalized degree of polymerization with the conversion between Model I and Model II.

Although there are little differences in the results for sample C between the two models, the difference in the shape of the curve for sample A should be recognized. The curve for sample A based on Model I shows a monotonic decrease in X/X_0 with a decrease in conversion for temperatures at 312°C and 360°C. However, the curve for sample A based on Model II initially shows a large drop in X/X_0 close to the 45° diagonal line followed by a slow drop in X/X_0 with a decrease in conversion away from the diagonal line. The experimentally determined relationships for sample A shown in Fig. 1 show exactly the same trend as calculated with Model II.

The relationship between the polydispersity of the sample residue and the conversion is calculated with Model II at the degradation temperature of 327°C for the three samples and the results are compared with those calculated with Model I. Figure 8 shows that the results calculated from Model II are not significantly different from those calculated from Model I and both calculated results agree reasonably well with experimental data.

TABLE I
Sample Material Characteristics

Sample	X_0	Polydispersity	Tacticity (%)			Manufacturer's designation ^a
			I	H	S	
A	315	1.1	4.8	38.8	56.4	PM4-1
B	1250	1.1	3.8	38.5	57.6	PM3-3
C	5 690	1.15	4.3	37.7	58.0	PM-33

^a Pressure Chemical Co., Pittsburgh, PA.

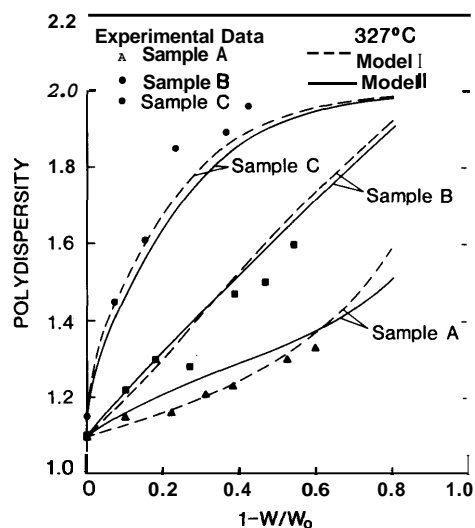


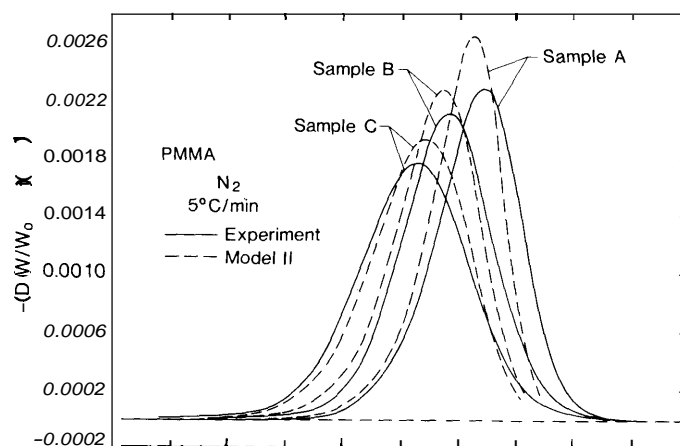
Fig. 8. Comparison of calculated change in polydispersity with the conversion at 327°C for the three samples with the experimental results (X_0 value **A**: 315, **B**: 1250, **C**: 5690).

In order to further examine the validity of the model, the theoretically calculated derivative thermogravimetry analysis, DTG, based on Model II is conducted for the three samples and their results are compared with the experimental data. Since the DTG analysis covers a wide range of temperatures, this examination might be more rigorous than that for an isothermal heating analysis. It is also important to demonstrate that the model calculation can be extended to dynamic heating which is becoming more common. The comparison of the DTG curves with the experimentally determined data is shown in Fig. 9. Both the theoretical and the experimental results show qualitatively that the maximum rate of degradation occurs at the higher temperature for the sample with smaller initial molecular weight and also that the peak value in weight loss rate decreases with the larger initial molecular weight. The difference in the temperature at the maximum rate of degradation between the calculated results and the experimental data is very small, a maximum of 4°C for sample **A**. This difference is much less than that calculated from Model I which is about 15°C. A detailed discussion of the effects of initial molecular weight on peak height and peak temperature is given in our previous work.¹

The activation energy of the global weight loss reaction is determined by the relatively simple but useful Kissinger's method.⁷ According to the expression derived by Kissinger:

$$\ln(\phi/T_m^2) = \ln(nRA(W_m)^{n-1}/E) - E/RT_m$$

where ϕ is the heating rate in the DTG analysis, T_m is the temperature at the



maximum rate of weight loss, A is the pre-exponential factor, W_m is the weight of the sample at the maximum rate of weight loss, and n is the apparent order of the reaction with respect to the sample weight. Experimentally determined values of T_m and theoretically calculated values of T_m based on the two models are listed in Table 2 for the three samples at different heating rates. The value of E can be determined from the slope of a plot of $\ln(\phi/T_m^2)$ versus $1/T_m$ at various heating rates without specifying the order of the reaction. Experimentally derived Kissinger plots for the three samples

TABLE 2
Temperatures at Maximum Weight Loss Rate (C)

ϕ ($^{\circ}\text{C}/\text{min}$)	Sample A		Sample B		Sample C				
	T_{me}	T_{mc}	T_{me}	T_{mc}	T_{me}	T_{mc}			
	Model		Model		Model				
	I	II	I	II	I	II			
5	379	368	375	367	359	365	356	355	359
3	373			361			350		
2	368	357	364	356	347	354	345	344	347
1	359	349	356	348	339	345	337	335	339
0.7	355	345	352	344	335	342	333	331	335
0.5	351	341	348	341	331	338	330	327	331

T_{me} : Experimental data

T_{mc} : Calculated results.

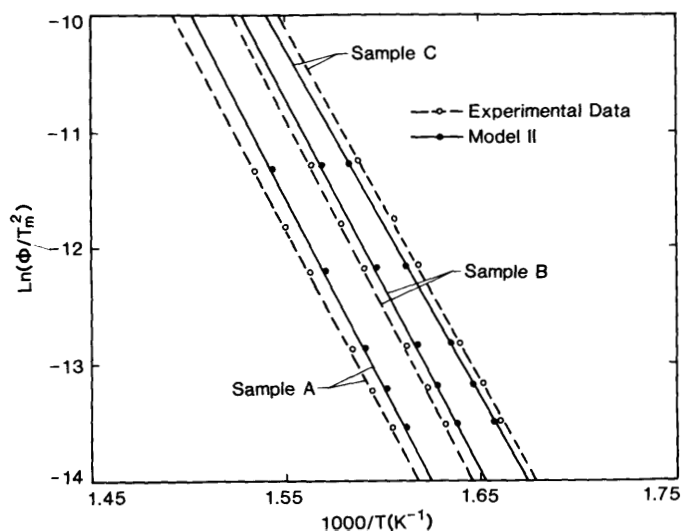


Fig. 10. Comparison of Kissinger plots of the three samples between the theoretical prediction and the experimental data (X_0 value **A**: 315, **B**: 1250, **C**: 5690).

are shown in Fig. 10 together with the theoretically calculated results based on the two models. The calculated results based on Model II agree with the experimental results much better than those based on Model I. The values of activation energy determined from a best fit of these plots are summarized in Table 3. The effects of initial molecular weight on the activation energy of the global weight loss reaction were discussed in detail in our previous study.¹ The accuracy of the results calculated by Model II is further demonstrated by comparing the calculated DTG curves with those determined by experiments for different heating rates. A typical comparison is shown in Fig. 11. The calculated DTG curves agree reasonably well with the experimental data over a wide temperature range for different heating rates.

It has been demonstrated that Model II can calculate: (1) a consistent value of Z for samples **A** and **C**, (2) the relationship between X/X_0 and

TABLE 3
Activation Energies of Global Weight Loss Reaction

Sample	Experimental data kJ/mol (kcal/mol)	Theoretical results kJ/mol (kcal/mol)	
		Model I	Model II
A	265 (63)	272 (64.9)	270 (64.5)
B	265 (63)	258 (61.6)	266 (63.6)
C	250 (60)	244 (58.4)	248 (59.2)

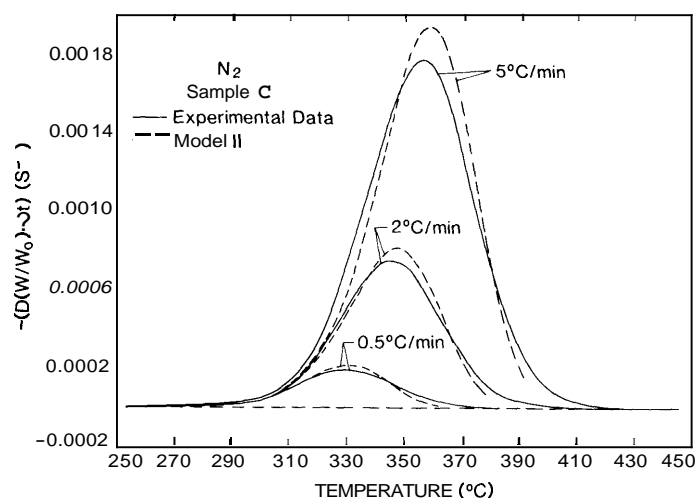


Fig. 11. Comparison of calculated DTG curves of sample C with experimental DTG curves—effects of heating rate.

conversion which agrees with the experimental data better than that calculated by Model I, and (3) the Kissinger plot and the DTG curve which agree with the experimental data better than those calculated by Model I. Therefore, the above results strongly suggest that depropagation from the primary radical during the thermal degradation of PMMA proceeds via the β scission as described by eqns (5) and (6) instead of the previously thought β scission at the backbone C—C bond (reaction scheme (1)). However, experimental proof at the occurrence of degradation products is required in order to show that the pathway is plausible. The unique degradation products from this degradation path are CO, CO₂, and possibly CH₄ and CH₃OH. It is expected that these products are not generated by reaction scheme (1). The experimental study to confirm the β scission described by eqns (5) and (6) is described in the next section.

EXPERIMENTAL APPARATUS

A schematic illustration of the experimental apparatus is shown in Fig. 12. A 25mm (ID) vycor tube with one closed end was connected to a Pyrex coil (2.4 m long) which was submerged in an ethanol dry-ice cold bath maintained at 198 K. The coil was connected to a quadrupole mass spectrometer. An auxiliary vacuum pump was plumbed in parallel with the mass spectrometer. The central portion of the vycor tube sat inside an insulated cylindrical furnace. Temperature inside of the furnace was monitored by a chromel/alumel thermocouple located on the outer portion of the vycor tube, inside the furnace.

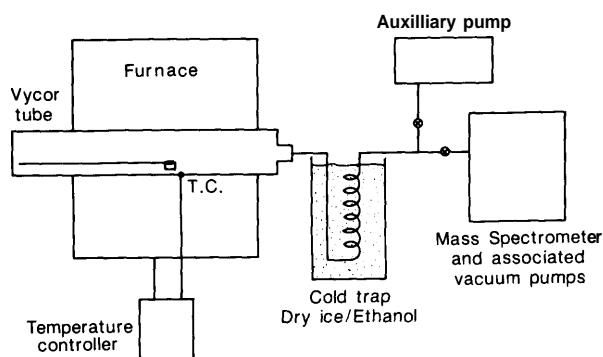


Fig. 12. Schematic illustration of the experimental set up for the products analysis.

Experimental procedure

Finely ground PMMA samples (3.0 ± 0.2 mg of A, B and C) held in a pre-baked aluminum dish was placed into the center of the vycor tube. The tube was evacuated by the auxiliary vacuum pump at room temperature. When the pressure was steady at about 1 millitorr the auxiliary pump was closed and the mass spectrometer was put on line. A pressure of 9.0×10^{-7} torr was achieved inside the mass spectrometer.

Methane, carbon monoxide, carbon dioxide and methyl methacrylate were observed at mass to charge ratios of 16, 28, 44 and 100, respectively. The measurement of methyl methacrylate was intended to test the collection efficiency of the cold trap. Methanol, another possible degradation product in the proposed degradation reaction path, was not measured because it was collected in the cold trap. Carbon monoxide was observed at an ionization energy of 14.8 eV. This ionization energy was chosen in order to avoid background signal from leaking ambient nitrogen whose ionization potential was 15.6 eV.⁸ The other species were observed at an ionization energy of 20 eV. The mass spectrometer and data collection functions were controlled by a microcomputer. The observed signal from the mass spectrometer was averaged for 5 s for each mass. Sets of masses were observed about every 30 s. Data collection was terminated after about 30 min when observed concentrations of CO and CO₂ became near zero.

The furnace heater was turned on and the temperature was monitored during the experiment. The time-temperature history in the furnace is shown in Fig. 13. It was identical for each of the samples studied, increasing monotonically from room temperature to about 420°C in 10 min and then being held constant. The pressure in the vycor tube was about 1 millitorr during the experiment.

A cold bath (198 K) was tested for its ability to trap CO₂. Carbon dioxide (50 ppm to 800 ppm) in nitrogen was measured by the mass spectrometer

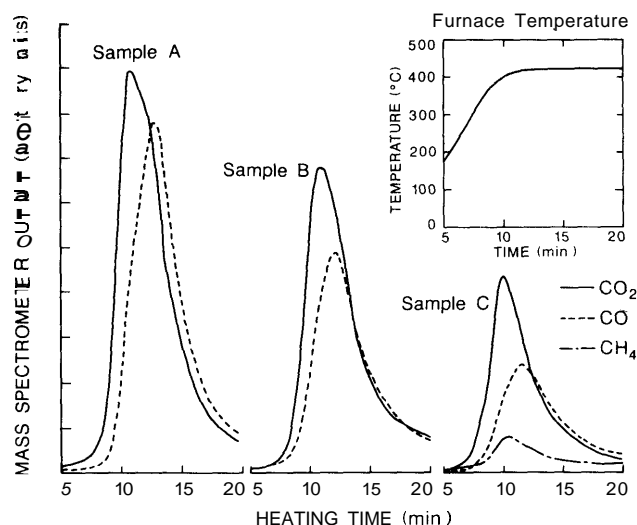


Fig. 13. Experimentally determined product measurement with heating time for the three samples (X_0 value **A**: 315, **B**: 1250, **C**: 5690).

with and without the cold trap in place. No diminution in mass spectrometer signal was observed with CO₂ passing through the cold trap.

In order to insure that the experimentally observed CO and CO₂ were not room temperature monomer fragments, a monomer sample was placed in the Pyrex tube and detected by the mass spectrometer without the cold trap in place. Copious quantities of monomer were detected but no CO or CO₂ signals were observed. Similar concerns regarding the possibility of CO₂ fragmentation leading to CO detection were negated by a value of the appearance potential of CO from a CO₂ source as 29 eV.⁸ This was experimentally verified by introducing CO, into the mass spectrometer at 14.8 eV and not being able to detect a CO fragment signal.

Calibration of the mass spectrometer for carbon dioxide, carbon monoxide, and methane was achieved by microprobe sampling of gas mixtures flowing at atmospheric pressure and room temperature.¹ Relative concentration ratios among the three gases were determined from the calibration.

EXPERIMENTAL RESULTS AND DISCUSSION

Typical mass spectrometer outputs for CO, CO, and CH, are plotted as a function of time after the start of heating of the furnace in Fig. 13. The furnace temperature history is also included to show how product concentrations change with temperature. The magnitude of each signal is

corrected by using the calibrated relative concentration ratios among the three gases. A limited number of CH_4 measurements were conducted to detect CH_4 in degradation products. As predicted by the proposed degradation path for the primary radical, all possible products of permanent gases are obtained. Furthermore, measured amounts of CO and CO_2 decrease with an increase in initial molecular weight of the sample, as expected from the proposed degradation path. According to the proposed pathway, with an increase in initial molecular weight, the incidence of the initial random scission which generates primary radicals decreases and CO and CO_2 concentration should also decrease. Since the possibility of termination exists during the degradation even for sample A ($X_0 = 315$) the peak heights of CO and CO_2 do not change linearly with initial molecular weight. The larger the initial molecular weight, the more termination tends to occur. Because more primary radicals may be generated, the peak height ratios among the three samples do not change quantitatively with initial molecular weight.

Yields of CO and CO_2 with respect to the initial **PMMA** sample are estimated by using the initial sample weight and by integration of CO and CO_2 signals of the mass spectrometer shown in Fig. 13. The volume flow rate through the tube is assumed to be equal to the capacity of the mass spectrometer turbo pump. Since the volume flow rate tends to become smaller with lower pressure, the yields may be overestimated. The CO and CO_2 yields are listed in Table 4. Since one random scission generates CO or CO_2 and many monomers by depropagation reaction before termination occurs, the inverse of the total yield (CO and CO_2) should be equal to the average zip length (actual length instead of kinetically determined length). For sample A, this value should be close to the initial degree of polymerization. The values listed are about 200 (about 100 each from CO and CO_2 , respectively) and the initial degree of polymerization of sample A is 315. With an increase in initial molecular weight, the probability of termination increases and this length tends toward the kinetically defined zip length (Z/X_0 , the average number of monomer units successively released by propagation initiated from one random scission along the length of polymer chain). As shown in Fig. 6, kinetically defined average zip lengths are about

TABLE 4
Yields of CO and CO_2 (mole ratio)

<i>Sample</i>	$\text{CO} \times 10^{-3}$	$\text{CO}_2 \times 10^{-3}$
A	8.7	10.0
B	5.3	7.6
C	3.6	4.1

1000–2000 depending on degradation temperature. The experimentally determined inverse of total yields are about 350 and 550 for samples **B** and **C**, respectively. Although the inverse of total yield is roughly a factor of two to three smaller than the kinetically defined average zip length, their agreement is quite reasonable considering the possibility of underestimation discussed above for the inverse of total yield value (overestimation for total yield).

It appears that the reaction path described by eqn (6) tends to occur slightly more often than that by eqn (5) and this trend becomes more pronounced with sample **C**. It is not clear why the peak ratio of CO/CO₂ decreases with an increase in the initial molecular weight and why the CH₄ concentration is much lower than that of CO₂. It is also interesting to notice that the CO₂ peak appears earlier (lower temperature) than the CO peak for all three samples. Although further studies are needed to clarify these points, it is clear that the proposed degradation paths described by eqns (5) and (6) are quite plausible.

CONCLUSION

A new degradation path from primary radicals generated from random scission of PMMA is proposed to describe the behavior of the primary radicals more correctly than the previously believed behavior of equal reactivity between the primary and tertiary radicals. This degradation path is via β scission at the pendant position instead of at the backbone position. The theoretical results clearly indicate that the formation of one polymer radical and one polymer molecule or the formation of one polymer molecule and another polymer molecule with an unstable bond cannot explain the experimentally determined relationship between degree of polymerization and conversion shown in Fig. 1.

The two degradation paths as described by eqns (5) and (6) are observed to be possible. The specific products evolved from the proposed degradation paths are experimentally measured and their peak values decrease with an increase in the initial molecular weight of the sample. The experimentally determined values of the inverse of the total yields of CO and CO₂ for samples with three different initial molecular weights agree reasonably well with average zip lengths. These results strengthen the plausibility of the proposed degradation paths.

ACKNOWLEDGMENT

We thank Dr Wing Tsang at Center for Chemical Physics of NBS for his valuable discussions and suggestions regarding degradation chemistry.

REFERENCES

1. Inaba, A., Kashiwagi, T. & Brown, J. E., Effects of initial molecular weight on thermal degradation of poly(methyl methacrylate) 1.—Model I. *Poly. Deg. and Stab.* (in press).
2. Guaita, M. & Chiantoe, O., *Poly. Deg. and Stab.*, **11** (1985) 167.
3. Guaita, M., Chiantoe, O. & Costa, L., *Poly. Deg. and Stab.*, **12** (1985) 315.
4. Kashiwagi, T., Inaba, A., Brown, J. E., Hatada, K., Kitayama, T. & Masuda, E., *Macromolecules*, **19** (1986) 2160.
5. Shampine, L. F., *Computer Solution of Ordinary Differential Equations*, W. H. Freeman and Company, San Francisco, 1975.
6. Wing Tsang, private communication.
7. Kissinger, H. E., *Anal. Chem.*, **29** (1957) 1702.
8. Levin, R. D. & Lias, S. G., Ionization Potential and Appearance Potential Measurements 1971–1981. US Department of Commerce Publication NSRDS-NBS 71, 1982.
9. Smyth, K. C., Miller, J. H., Dorfman, R. C., Mallard, W. G. & Santoro, R. J., *Combust. and Flame*, **62** (1985) 157.
10. Inaba, A. & Kashiwagi, T., *Macromolecules*, **19** (1986) 2412.

APPENDIX: THEORETICAL MODEL BASED ON REACTION SCHEME (2)

As described in the section above headed ‘Probable Behavior of the Primary Radical’, initiation reaction of this model is:



The same reactions of depropagation and termination and the same approximation as in Models I and II are also used in this model as described in the paper. The governing equations are:

$$d[M_n]V/d\tau = -(n-1)[M_n]V + \sum_{i=n+1}^{\infty} [M_i]V + \frac{1}{Z'} [R_n]V \quad (\text{A-1})$$

$$d[R_n]V/d\tau = \frac{Z}{Z'} ([R_{n+1}] - [R_n])V + \sum_{i=n+1}^{\infty} [M_i]V - \frac{1}{Z'} [R_n]V \quad (\text{A-2})$$

$$d[R_1]V/d\tau = \frac{Z}{Z'} [R_2]V + 2M_0V - \frac{1}{Z'} [R_1]V \quad (\text{A-3})$$

where

$$\begin{aligned} \mathbf{M}_0 &= \sum_{n=2}^{\infty} [M_n] & \mathbf{M}_1 &= \sum_{n=2}^{\infty} n[M_n] \\ \mathbf{M}_2 &= \sum_{n=2}^{\infty} n^2[M_n] & \mathbf{R}_0 &= \sum_{n=1}^{\infty} [R_n] \end{aligned} \quad (\text{A-4})$$

The numerical solution of the above equations is conducted for various values of X_0 , Z/X_0 and P_0 and also with different orders of the termination reactions. Typical results are plotted in Fig. 2. Different values of P_0 and a different order of termination reactions do not make any significant changes in the results shown in Fig. 2.

Using the assumption of a steady-state radical concentration, the following equation can be derived from the summation of eqn (A-2) with eqn (A-3):

$$\mathbf{R}_0 = Z'\mathbf{M}_1 \quad (\text{A-5})$$

Using eqn (A-4) and eqn (A-5), eqn (A-1) can be written as:

$$(1 - Z)d\mathbf{M}_0V/d\tau - d\mathbf{M}_1V/d\tau = \mathbf{M}_1V + (Z - 1)\mathbf{M}_0V \quad (\text{A-6})$$

With the assumption of a steady-state radical concentration, the value of the radical concentration can be derived from eqn (A-1) and the steady-state form of eqn (A-2) as:

$$[R_n] = \frac{Z'}{(1 + Z)} \sum_{j=n+1}^{\infty} \left[\frac{(Z)^{j-(n+1)}}{(1 + Z)} \sum_{i=j}^{\infty} [M_i] \right] \quad (\text{A-7})$$

With the same approximation as used in our previous study (eqn (36)),¹⁰ eqn (A-1) becomes:

$$\frac{d\mathbf{M}_0V}{d\tau} = -\mathbf{M}_0V + \frac{\mathbf{M}_1V}{1 + 2Z(\mathbf{M}_1/\mathbf{M}_2)} \quad (\text{A-8})$$

By definition

$$\begin{aligned} X &= \mathbf{M}_1/\mathbf{M}_0 \\ S &= (\mathbf{M}_2\mathbf{M}_0)/(\mathbf{M}_1\mathbf{M}_1) = \mathbf{M}_2/(\mathbf{M}_1X) \end{aligned}$$

Then, eqn (A-6) becomes:

$$\begin{aligned} (1 - Z)d(V/X)/d\tau - dV/d\tau &= V + (Z - 1)(V/X) \\ (1 - Z)d(V/X)/d\tau &= \left[-1/X + \frac{1}{1 + 2Z/PX} \right] V(1 - Z) \end{aligned} \quad (\text{A-9})$$

From these equations, the following equations can be derived:

$$-dV/d\tau = ZSXV/(SX + 2Z) \quad (\text{A-10})$$

$$dX/d\tau = -X^2S(X + Z)/(SX + 2Z) \quad (\text{A-11})$$

By dividing eqns (A-10) and (A-11) by X_0 , for the limit of $Z/X_0 \rightarrow \infty$ the above equation becomes:

$$dV/d(X/X_0) = V/(X/X_0)$$

The solution to this equation is:

$$V = (X/X_0) \quad \text{or} \quad 1 - V = 1 - (X/X_0)$$
